THE JOURNAL OF PHYSICAL CHEMISTRY C
A JOURNAL OF THE AMERICAN CHEMICAL SOCIETY

pubs.acs.org/JPCC

Article

Biruthenium Complexes for Semiconductor Functionalization: Insights into Surface Binding and Charge Separation on TiO_2(110)

Luciano Sanchez Merlinsky, Bruno M. Aramburu-Trošelj, Carolina Pistonesi, M. Estela Pronsato, Luis Baraldo, and Federico J. Williams*

Cite This: https://doi.org/10.1021/acs.jpcc.5c01952

Read Online

ACCESS | Metrics & More | Article Recommendations | Supporting Information

ABSTRACT: We investigated the adsorption and electronic properties of a cyanide-bridged biruthenium complex on rutile TiO_2 (110) surfaces using X-ray photoelectron spectroscopy (XPS) and density functional theory (DFT) calculations. This dimer complex forms a stable monolayer on the surface, with a bidentate binding through deprotonated carboxylic acid groups, similar to its monomeric counterparts. DFT calculations of the [II,II] complex suggest that the energy of the lowest unoccupied molecular orbital (LUMO) overlaps with the conduction band of TiO_2, facilitating electron injection from the excited state of the complex. For the mixed-valence complex, both spectroscopy and DFT predict that the hole is localized on the distal ruthenium center, which is spatially separated from the TiO_2 interface, potentially reducing the rate of back electron transfer. Our findings offer new insights into the interaction of biruthenium complexes with TiO_2, contributing to the development of advanced molecular systems for light-driven applications such as dye-sensitized solar cells and photocatalysis.

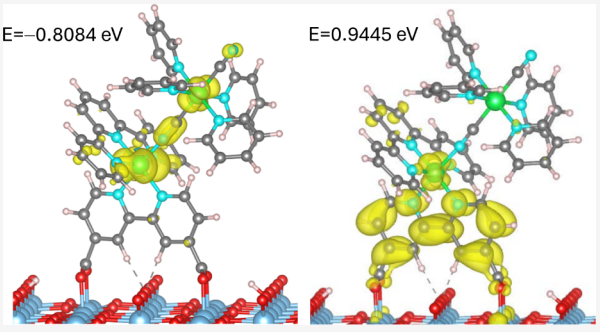

INTRODUCTION

Incorporating molecules onto semiconductor surfaces is a promising strategy to introduce new functionalities, broadening their range of applications. Key functionalities include light sensitization across the visible spectrum,[1,2] targeted reactivity and molecular sensing[3] and drug delivery.[4] Coordination complexes, such as those used in dye-sensitized solar cells (DSSCs),[5] are particularly attractive for this purpose due to their tunable light absorption properties. By designing complexes that enhance visible light absorption, semiconductors can be sensitized to energies lower than their band gap when these complexes are anchored to their surfaces.

In DSSCs, the primary processes involve: a) light absorption, where excited states centered on the molecule inject electrons into the semiconductor's conduction band, and b) regeneration of the oxidized molecule via a redox mediator, which restores the cycle. The efficiency of this process can be improved by incorporating multiple redox centers in the chromophore, leading to longer-lived charge-separated states. This minimizes recombination of the injected electron with the oxidized molecule before it is regenerated, a key step for efficient photoanode performance.[6]

Cyanide-bridged biruthenium polypyridyl complexes are particularly suited for this application due to their high electronic coupling and low reorganization energies, enabling electron delocalization at room temperature.[7,8] These properties enhance the formation of mixed-valence states, where fast inner-sphere electron transfer is crucial to outpace detrimental recombination processes. The photophysical properties of ruthenium polypyridyl oligomers have been also studied, with a focus on their ability to absorb light across various regions of the visible spectrum, which can involve charge transfer transitions between their monomeric fragments.[7−10] Moreover, inspired by natural photosynthetic systems, these complexes are being explored as potential catalysts for collecting and storing electrons in reaction centers capable of driving catalytic processes, such as water oxidation.[11,12]

Density functional theory (DFT) calculations offer valuable insights into the electronic structure and spectroscopic behavior of these complexes, particularly in relation to their redox states. However, challenges arise in calculating mixed-valence systems, where delocalized electronic configurations are often underestimated due to the self-interaction error inherent in most DFT functionals.[13] Despite these limitations, DFT remains a powerful tool for probing the structure, electronic properties, and electron transfer mechanisms of ruthenium complexes adsorbed on semiconductor surfaces,

Received: March 23, 2025
Revised: June 11, 2025
Accepted: June 12, 2025

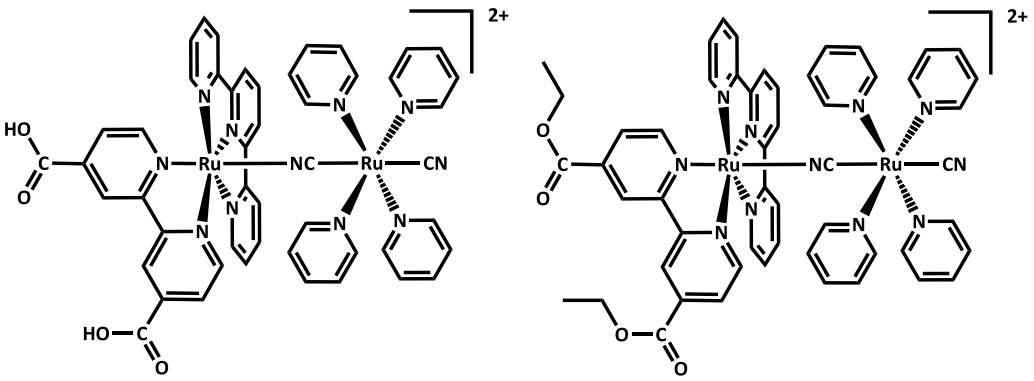

Figure 1. Molecular structures of the complexes studied in this work; cyanide bonds and H atoms are omitted for clarity. The Ru fragment with the terpyridine ligand is labeled Ru_{pp} and the one with pyridine ligands is labeled Ru_{py}.

such as TiO_2. Notably, DFT calculations can predict the binding geometry, as well as the relative energies of the highest occupied and lowest unoccupied molecular orbitals (HOMO and LUMO), providing insights into the viability of interfacial electron transfer.[14−16]

The interaction between ruthenium complexes and TiO_2 has been the focus of extensive research, particularly through photoemission spectroscopies, due to its significance in photoinduced charge transfer reactions and applications such as dye-sensitized solar cells. Previous studies have examined the adsorption of Ru polypyridine complexes on nanostructured TiO_2,[17−22] as well as on well-defined TiO_2(110) single crystal surfaces.[23−25] These measurements elucidate the binding modes, molecular structures, and adsorption geometries of the complexes, while also providing insights into the energy level alignment between the dyes and the TiO_2 substrate. Notably, to our knowledge, there are currently no reports on the interaction of biruthenium complexes with TiO_2 surfaces. In contrast, the interaction of ruthenium dimers adsorbed on alkanethiol self-assembled monolayers on gold surfaces has been investigated using X-ray Photoelectron Spectroscopy (XPS).[26] In this context, the monocationic mixed-valence species $[((acac)_2Ru)_2bptz]^+$ displays a single set of XPS binding energies for the Ru 3d and 3p orbitals, suggesting that both Ru atoms in the dimer share the same oxidation state, indicative of significant charge delocalization within this compound.

In this work, we synthesized a cyanide-bridged biruthenium complex, in which one ruthenium center bears two carboxylic acid groups for attachment to metal oxide surfaces (see Figure 1). The Ru fragment with terpyridine and dicarboxy-bipyridine ligands is labeled Ru_{pp}, whereas the Ru fragment with the four pyridine ligands is labeled Ru_{py}. We studied the dimeric complex's behavior in solution, focusing on its redox states. Furthermore, the complex was deposited onto rutile TiO_2(110)−(1 × 1) single crystal surfaces. X-ray photoelectron spectroscopy (XPS) measurements and DFT calculations reveal that the biruthenium complex forms a stable monolayer on the TiO_2 surface and that upon one-electron oxidation, the resulting hole is localized on the distal ruthenium center, away from the semiconductor surface.

METHODS

We synthesized and characterized the Ru complexes as detailed in the Supporting Information. Rutile TiO_2 (110) single crystals were obtained from CrysTec GmbH. Solvents used for spectral, electrochemical, and photoelectronic measurements were purified following the established procedures.[27,28] All other synthesis materials were of reagent grade and obtained commercially without further purification. Before characterization, all complexes underwent a minimum of 24 h of vacuum desiccation.

Spectroelectrochemical measurements in the UV−visible region were performed with a Honeycomb electrode array from PINE Research Instrumentation, equipped with a Pt working electrode, a Pt counter electrode and a Ag wire pseudoreference electrode. A WaveNowXV potentiostat from PINE Research Instrumentation was coupled with an Avantes AvaLight DHc light source and an Avantes AvaSpec-2048 spectrometer, to record each spectrum at a given applied potential. Near-infrared (NIR) spectroelectrochemistry was carried out on a Shimadzu UV-3101PC spectrometer with an OTTLE cell.[29] All electrochemical and spectroelectrochemical measurements used acetonitrile 0.1 M $TBAPF_6$ as electrolyte solution, with a millimolar solution of the complex. The IR spectrum of the sample in a KBr pellet was obtained with a Nicolet iS10 FT-IR spectrometer (range 11 000−400 cm^{-1}). ^1H NMR spectral data were acquired with a Bruker ARX500 spectrometer, using deuterated solvents from Aldrich. The cyclic voltammetry was measured in a TEQ 04 potentiostat, using a standard three-electrode array consisting of a glassy carbon disc (area = 9.4 mm^2) as the working electrode, a platinum disc as the counter electrode and a silver wire as the pseudoreference electrode, plus an internal ferrocene (Fc) standard. A scan rate of 100 mV s^{-1} was employed. All potentials reported here were referenced to the standard Ag/AgCl (saturated KCl) electrode (0.197 V vs. NHE), with the conversions according to reported literature values for the Fc^+/Fc couple.[30]

Density Functional Theory (DFT) computations were employed to fully optimize the geometries of the esterified complex in vacuum and acetonitrile, without symmetry constraints. The geometries of the singlet ground state were optimized and serve as the starting point for the optimization of the oxidized species. DFT calculations were performed with Gaussian09[31] at the B3LYP level of theory using restricted and unrestricted approximations of the Kohn−Sham equation, depending on the total number of electrons.[32] In all cases, we employed the effective core potential basis set LanL2DZ, which has proven suitable for geometry predictions in coordination compounds containing second-row transition metals and allows for a direct comparison with previous

https://doi.org/10.1021/acs.jpcc.5c01952
J. Phys. Chem. C XXXX, XXX, XXX−XXX

calculations.[8] Solvation effects were accounted for using the most recent implementation of the implicit IEF-PCM solvation model.[33,34] All optimized structures were confirmed as minima by analyzing the harmonic vibrational frequencies.[35] Vertical electronic excitation energies and intensities were evaluated using the time-dependent DFT (TD-DFT)[36,37] under the linear response formalism, without symmetry constraints, for the first $N = 100$ excited states for Ru(II)−Ru(II), $N = 150$ for MV, and $N = 200$ for Ru(III)−Ru(III). Note that, in general, TD-DFT-calculated transitions with oscillator strengths greater than 0.1 are selected; however, when predicting IVCT bands, we also consider symmetry-forbidden transitions with lower oscillator strengths. GaussSum 3.0 software[38] was used to perform spectral simulations, extract spectral data and molecular orbital information and to obtain electron density difference maps (EDDMs) and spin densities of the oxidized species. Graphical visualizations were performed using GaussView 6.0.16. Data of the most relevant EDDMs, the composition of the electronic transitions and the associated molecular orbitals of the calculated complex are shown in the Supporting Information.

XPS measurements were conducted in an ultrahigh vacuum (UHV) chamber with a base pressure below 5×10^{-10} mbar using a SPECS spectrometer system equipped with a 150 mm mean radius hemispherical electron energy analyzer and a nine channeltron detector. XPS spectra were obtained on grounded conducting substrates at a constant pass energy of 20 eV using a monochromatic Al Kα (1486.6 eV) X-ray source operated at 15 kV and 20 mA at a detection angle of 20° with respect to the sample normal. For the adsorbed complex on TiO_2 (110), binding energies of the Ti 2p and O 1s regions were aligned to the substrate Ti $2p_{3/2}$ signal at 459 eV,[39] while the C 1s−Ru 3d and N 1s regions were referenced with respect to the aliphatic C 1s signal at 285 eV.[40] Prior to each experiment, the rutile TiO_2 (110) single crystal was cleaned by several cycles of Ar^+ sputtering and annealing until no impurities were detected by XPS. Deposition of the Ru dimer containing carboxylic acids on the TiO_2 (110) surface was carried out in an argon-filled liquid cell attached to the UHV chamber.[30] The clean TiO_2 (110) crystal was dipped in a 10^{-4} M methanolic solution of the ruthenium polypyridine dimer at room temperature for 1 h without exposure to the laboratory atmosphere. Afterward, the crystal was removed from the solution, rinsed with methanol (3 × 10 mL) and dried with Ar. The sample was then transferred from the argon atmosphere to the UHV chamber for measurements.

The Vienna Ab-Initio Simulation Package (VASP) was employed to perform the DFT calculations of the adsorbed complex on the TiO_2 (110) surface, using a plane-wave basis set and a periodic supercell method.[41−43] Potentials within the projector augmented wave (PAW) method[44] and gradient-corrected functionals in the form of the generalized-gradient approximation (GGA) with Perdew Burke Ernzerhof (PBE) functional[45] were used. Van der Waals interaction between pairs was included using the Grimme DFT-D2 method.[46] For all calculations, a kinetic energy cutoff of 400 eV was employed and the strong electron correlation effects of the Ti 3d electrons were described by a Hubbard-type on-site Coulomb repulsion using the DFT + U Duradev's approach with an effective U value of 10 eV.[47] The rutile TiO_2(110)−(1 × 1) surface was modeled with a slab containing three Ti layers and 3 × 6 surface unit cells, which results in a 1.97 × 1.79 × 0.93 nm supercell (see Figure S5). The slab size ensures that there is no interaction between adsorbed molecules. Lattice parameters obtained from bulk optimization were used to build the slab. The first Ti layer with all its neighboring O ions was allowed to fully relax, while the bottom layers of the slab were fixed to their bulk positions. A vacuum gap of approximately 3.0 nm was employed to avoid interactions with neighboring slabs. For geometry optimization of the adsorbate on the surface, the ruthenium complex adsorbate was allowed to fully relax as well as the first Ti layer, including all its neighboring O ions. A cut condition of 10^{-3} eV for the total energy between two ionic relaxation steps was considered. The electronic relaxation convergence criterion was set to 10^{-4} eV and a set of 3 × 3 × 1 Monkhorst−Pack k-points was used.[48] Total density of states (TDOS) and projected density of states (PDOS) curves were used to analyze the electronic structure. In this case, a 7 × 7 × 1 k-points grid was employed.

RESULTS AND DISCUSSION

Cyclic voltammetry (CV) offers a powerful approach for studying charge transfer, revealing recombination processes, intrinsic symmetry constraints, and energy levels of active materials.[49] Note that CV measurements in solution were carried out using the ester-derivatized form of the dimer complex, as this avoids complications from multiple acid−base conjugate pairs affecting redox properties and closely resembles the carboxylate form bound to TiO_2. Figure 2

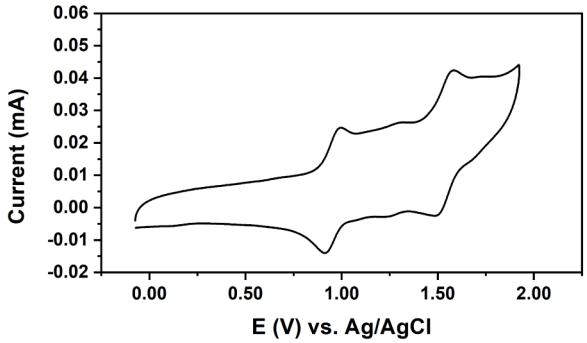

Figure 2. Cyclic voltammogram of the Ru esterified dimer in acetonitrile.

shows the CV of the ester complex, displaying two quasi-reversible anodic waves corresponding to oxidation processes at the two Ru centers. Like other Ru cyanide-bridged polypyridine complexes, the position of these redox signals reflects the chemical environment, which can be modulated by ligand substitution.[8] In this case, the oxidation of the Ru_{py} fragment occurs at 0.95 V, while the Ru_{pp} fragment oxidizes at 1.54 V (vs Ag/AgCl), attributed to the strong electron-accepting properties of the polypyridine ligands, further enhanced by the ester group's presence and its greater degree of conjugation compared to pyridine ligands. The one-electron oxidation leads to the formation of a cyanide-bridged mixed-valence (MV) complex. Assigning the electronic configuration of such complexes is challenging, as they may exhibit localized (Class II) or delocalized (Class III) electronic states.[50,51] However, as discussed below, spectroelectrochemical studies and DFT calculations aid in determining the electronic structure. The electronic configuration of the MV redox state is highly relevant in the context of photoinduced single-electron transfer from the surface-bound complex to the

https://doi.org/10.1021/acs.jpcc.5c01952
J. Phys. Chem. C XXXX, XXX, XXX−XXX

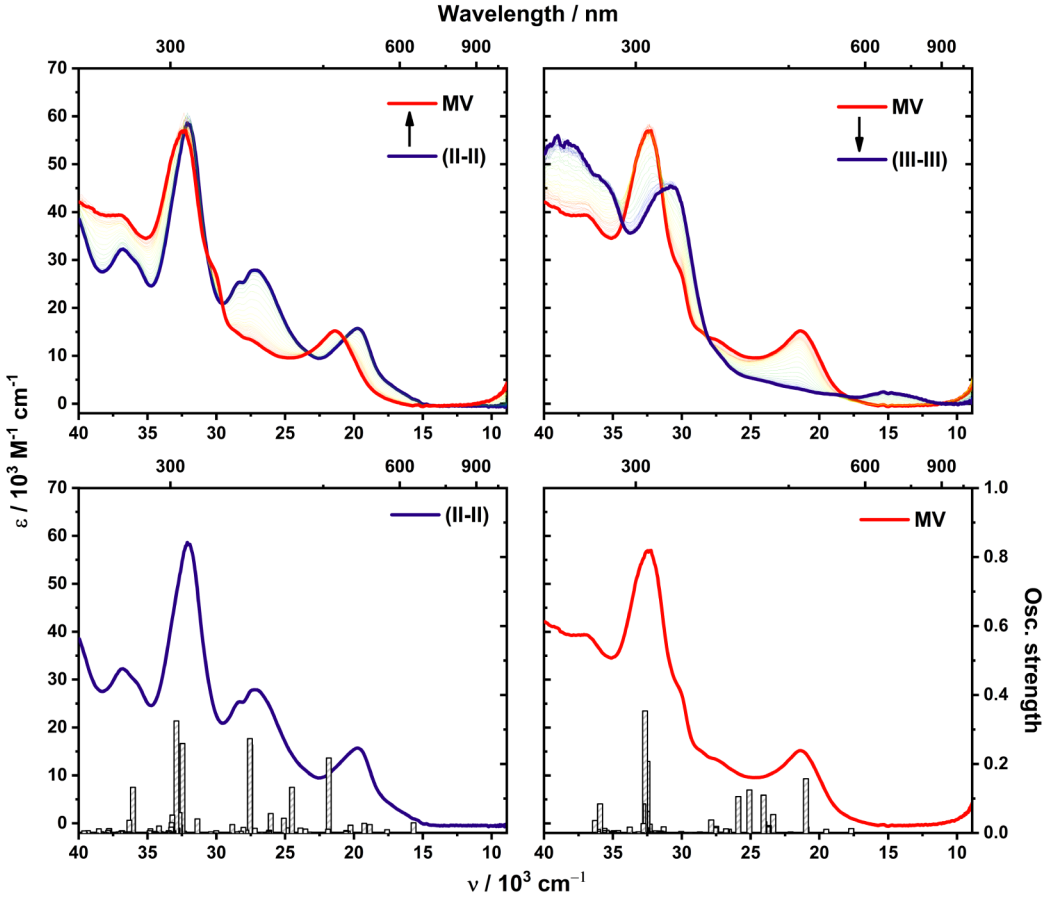

Figure 3. Top: UV−vis spectroelectrochemistry of the esterified complex in acetonitrile during the first (left) and second (right) oxidation processes. The spectra of the [II,II] and [III,III] species are highlighted in violet, while the mixed valence (MV) species spectrum is shown in red. Bottom: comparison of the experimental UV−vis spectra of the [II,II] and the mixed valence species in acetonitrile and the expected transitions obtained by TD-DFT calculations (bars).

semiconductor's conduction band. The position (distance)[52] and orientation (orbital overlap)[53] of the hole generated in the MV complex influence the rate of back-electron transfer from the semiconductor to the MV complex, thereby affecting the overall electron transfer efficiency.

The top of Figure 3 presents the UV−vis absorption spectra of the [II,II], mixed-valence (MV), and [III,III] species of the Ru dimer. The [II,II] species shows two distinct metal-to-ligand charge transfer (MLCT) bands, primarily attributed to $d\pi(Ru_{pp}) \rightarrow \pi^*(tpy/deeb)$ and $d\pi(Ru_{py}) \rightarrow \pi^*(py)$ transitions, located at 20,000 cm^{-1} and 27,000 cm^{-1}, respectively. Additionally, strong ligand-centered (LC) $\pi \rightarrow \pi^*$ transitions within the polypyridine ligands, mixed with MLCT $d\pi(Ru_{pp}) \rightarrow \pi^*(tpy)$ transitions, are observed at 32,000 cm^{-1} and higher. Upon one-electron oxidation, the $d\pi(Ru_{py})$ transitions are bleached, indicating that the oxidation is centered at the Ru_{py} site, as confirmed by TD-DFT calculations (see below). The transitions related to the $d\pi(Ru_{pp})$ orbitals shift slightly toward the blue (~1300 cm^{-1} for the lower MLCT band), likely due to the stabilization of the $d\pi(Ru_{pp})$ orbitals resulting from their interaction with the oxidized Ru_{py} center. Further oxidation to the [III,III] species leads to the disappearance of the remaining $d\pi(Ru_{pp})$ MLCT band, with a new band appearing at 15,000 cm^{-1}, which is assigned by TD-DFT to a ligand-to-metal charge transfer (LMCT) transition, specifically $\pi(tpy/py) \rightarrow d\pi(Ru_{pp/py})$ (see Figures S6 and S12). The bottom of Figure 3 shows a comparison of the experimental UV−vis spectra of the [II,II] and the mixed valence species in acetonitrile and the expected transitions obtained by TD-DFT calculations (bars). The calculated transitions reproduce the experimental measurements, allowing to assign the contributions for each band, including the MLCT, LC, and LMCT transitions in all cases (see Figures S6, S7, S9 and S12).

Figure 4a shows the near-infrared (NIR) absorption spectra of the [II,II], mixed-valence (MV) and fully oxidized species of the dimeric complex. In the MV species, the spectrum is dominated by an intervalence charge transfer (IVCT) band centered at 6700 cm^{-1}, absent in the reduced and oxidized forms. This band arises from electronic transitions in which the hole is predominantly localized at the $Ru_{py}(III)$ center, acting as the acceptor (A), while the $Ru_{pp}(II)$ center serves as the donor (D). The IVCT band exhibits an asymmetrical shape, skewed toward the lower energy region, with a shoulder at 5200 cm^{-1}. These features are influenced by the extent of the electronic coupling (H_{ab}) between the donor and acceptor, the splitting of the t_{2g} orbitals of both D and A centers into Kramers doublets due to spin−orbit coupling, and the low symmetry of the Ru_{pp} fragment.[51] Ultimately, the IVCT band results from the convolution of multiple intervalence charge transfer transitions originating from donor states with varying energies,[51] as it has been previously observed in carboxylate-free analogous cyanide-bridged bimetallic Ru complexes.[8] Figure 4b displays the NIR spectrum of the MV redox state

https://doi.org/10.1021/acs.jpcc.5c01952
J. Phys. Chem. C XXXX, XXX, XXX−XXX

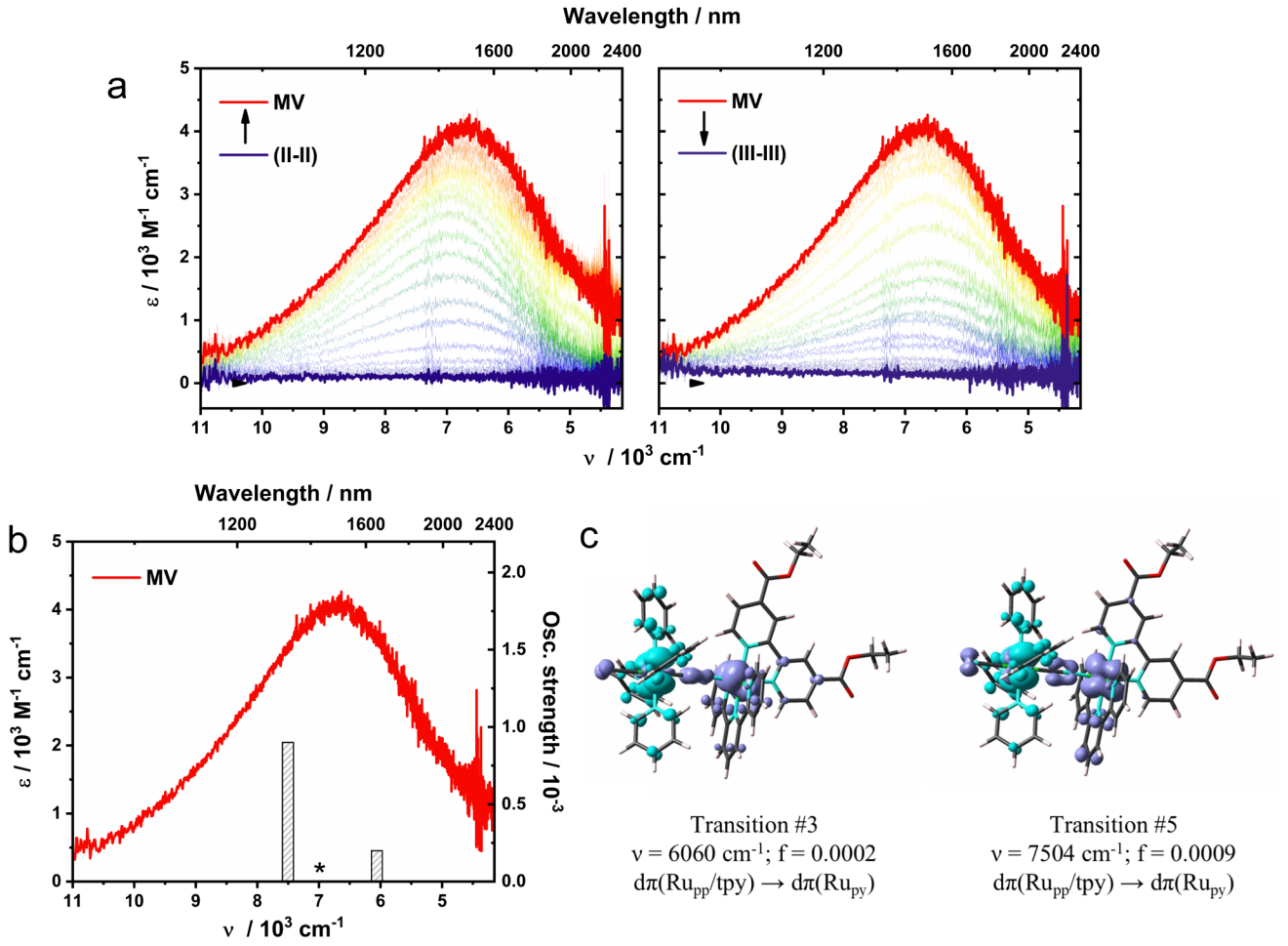

Figure 4. (a) NIR spectroelectrochemistry of the esterified complex in acetonitrile during the first (left) and second (right) oxidation processes. The spectra of the [II,II] and [III,III] species are highlighted in violet, while the mixed valence (MV) species spectrum is shown in red. (b) Comparison of the experimental NIR spectrum of the mixed valence species in acetonitrile and the expected transitions obtained by TD-DFT calculations (bars). A calculated transition with an oscillator strength equal to zero is marked with *. (c) TD-DFT-simulated EDDMs for the IVCT transitions in the NIR region, including their energy (ν) and oscillator strength (f). Orbitals where electronic density is increased and decreased after the transition are shown in light blue and purple, respectively.

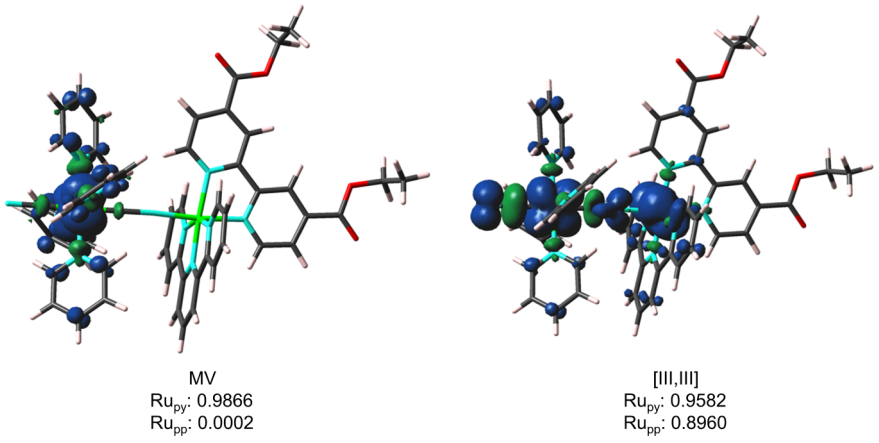

Figure 5. DFT-computed spin density (top) and Mulliken spin densities (bottom) for the mixed valence (left) and [III,III] (right) species in acetonitrile.

and the TD-DFT calculated transitions (bars). DFT calculations predict transitions at 7500 cm^{-1} and 6000 cm^{-1}, as well as a symmetry-forbidden transition at 7000 cm^{-1} that may contribute to the spectrum via vibronic and spin−orbit coupling effects. The calculated transitions align with the measured spectrum validating the computed configuration of the complex and confirming that the hole is distal from the anchoring site. Figure 4c shows the electron density difference

https://doi.org/10.1021/acs.jpcc.5c01952
J. Phys. Chem. C XXXX, XXX, XXX−XXX

maps (EDDMs) of the IVCT transitions, where the acceptor orbital has a major contribution from the LUMO β molecular orbital, located on the Ru_{py} center, and the donor orbitals are $d\pi$ orbitals located along the bridge and extended over both Ru centers (H-5β, H-4β, H-2β, H-1β and HOMO β MOs, see Table S3), hence overlapping with each other. This explains the relatively strong intensity observed for these transitions.

Figure 5 shows the DFT-calculated spin density and Mulliken spin densities for the mixed valence (left) and [III,III] (right) species in acetonitrile. This shows a complete localization of the hole on the Ru_{py} fragment in the MV species, with a major contribution of the $d\pi_{xy}(Ru_{py})$ orbital to the LUMO, which is in the plane lying perpendicular to the cyanide bridge. This is due to the higher basicity of the py ligand, and hence we expect a similar configuration for the complex bound to the surface. As mentioned above, if the dimer binds to the semiconductor surface through the carboxylic acid functional groups, then the localization of the LUMO distant from the surface should result in a slower rate for back-electron transfer, since the reorganization energy (thus the activation barrier) for interfacial electron transfer increases when the acceptor is placed at longer distances from the surface, regardless of the environment.[54]

An interesting feature of the herein synthesized binuclear complex resides in the fact that the donor excited state and the acceptor MV state are located at convenient distances for fast electron injection for the former, and slow recombination for the latter. The excited state is localized in the Ru_{pp} moiety, which can be formally described as an MLCT $\{Ru^{III}(tpy^{\cdot-})\}$ state,[55] (refer below to TD-DFT calculations), which is placed close to the surface. This accelerates the electron injection rate, whereas the accepting MV redox state places the acceptor moiety far from the surface, slowing down recombination. Therefore, considering the structural advantages this system presents, we focus in determining the complex molecular adsorption geometry on TiO_2 (110) surfaces.

Figure 6 shows the Ti $2p_{3/2}$, O 1s, C 1s−Ru 3d and N 1s XPS spectra for both the clean TiO_2 (110) crystal (black lines) and the adsorbed complex (red lines), with the Ti $2p_{3/2}$ signal referenced at 459 eV due to Ti^{4+}. For clarity, the intensity of the initial TiO_2 (110) surface spectrum was scaled by a factor of 0.5. Note that the Ti $2p_{3/2}$ XPS spectrum of the clean surface exhibits a shoulder at 457 eV due to Ti^{3+}, which accounts for approximately 5% of the total intensity. As the photoelectrons arising from the substrate pass through the adsorbed molecular layers, they suffer inelastic processes, leading to the attenuation of the Ti 2p and O 1s signals from the TiO_2. Surface coverage can be estimated using the inelastic mean free path from studies of similar systems, such as adsorbed porphyrins on TiO_2 (110) crystals.[56] The result indicates that the Ru dimer is deposited with a coverage of 0.49 ML. Note that we cannot rule out the coadsorption of methanol molecules, which would result in only a slightly lower calculated surface coverage for the dimer complex due to methanol's much shorter molecular length. Furthermore, the Ru $3d_{5/2}$ intensity of the adsorbed dimer complex is twice that of 0.5 ML of the adsorbed monomer complex $[Ru(tpy)(dcb)\text{-}NCCH_3]^{2+}$ (Figure S15), indicating similar coverages.[23] The P 2s and F 1s XPS regions show no signals, indicating the absence of PF_6^- adsorption, which is consistent with the adsorption of the fully deprotonated complex with a net zero charge.[57] The O 1s XPS signal from the substrate is present at 530.2 eV. After the adsorption of the biruthenium complex, a

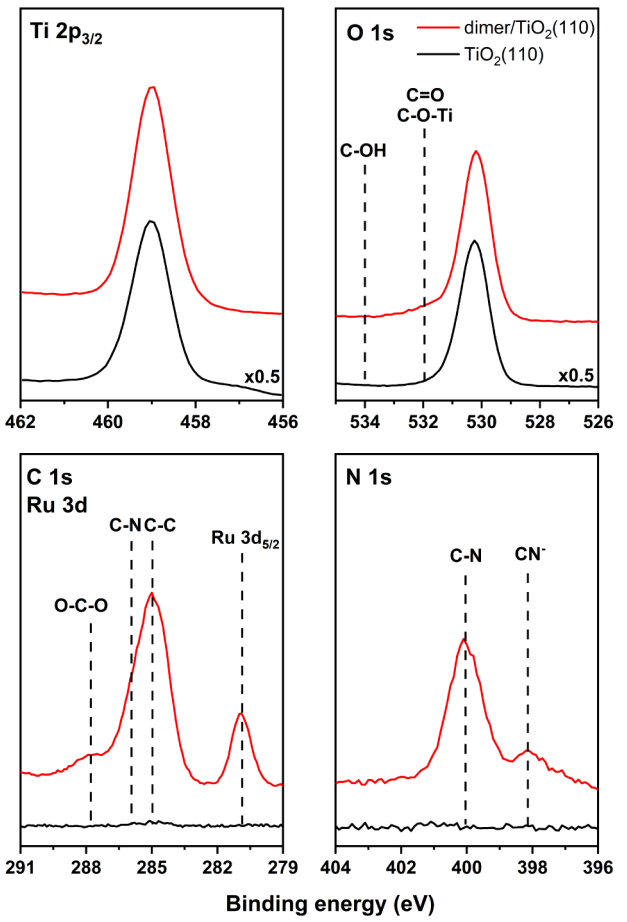

Figure 6. Ti $2p_{3/2}$, O 1s, C 1s−Ru 3d, and N 1s XPS spectra of the clean substrate (black lines) and the adsorbed biruthenium complex functionalized with carboxylic acid groups on TiO_2 (110) (red lines).

shoulder appears at 532 eV and is attributed to Ti−OH, −C−O−Ti, and −C═O groups.[56] Note that overlapping this peak, there could be a minor shakeup satellite. No contribution from −C−OH from the carboxylic acids is observed at 534 eV, confirming deprotonation of both linker groups and suggesting adsorption through both carboxylates in a bidentate manner. This is consistent with previous reports of carboxylate groups binding to TiO_2 (110) surfaces.[58,59]

Note that the absence of C and N in the initial substrate confirms the surface cleanliness before the deposition of the complex. The spectra of the adsorbed complex show all the expected features previously reported for Ru(II) complexes,[19,22,23,60] with a C 1s broad signal at 285 eV and the Ru $3d_{5/2}$ peak located at 280.9 eV. Note that the Ru $3d_{3/2}$ peak directly overlaps with the C 1s peak as the spin-orbit coupling is 4.2 eV. The biruthenium complex displays a single Ru $3d_{5/2}$ XPS peak, likely due to electronic coupling between the Ru centers.[26] Notably, DFT calculations show delocalization of the HOMO, H-1, H-3, and H-5 molecular orbitals over the cyanide bridge and both Ru centers (see Figure S8), providing further evidence of electronic coupling. Additionally, the Ru $3d_{5/2}$ peak of the dimer appears at a binding energy intermediate between those of its individual monomeric components (see Figure S16). The O—C—O and the shake-up satellite signals associated with molecules with extended π systems, are located within the shoulder at around 287.8 eV. Two peaks are observed in the N 1s region, the high

https://doi.org/10.1021/acs.jpcc.5c01952
J. Phys. Chem. C XXXX, XXX, XXX−XXX

binding energy peak at 400 eV is due to the N atoms present in the pyridine and polypyridine ligands, whereas the low binding energy peak at 398.1 eV is due to the cyanide ligand.[61] Their intensity ratio is 2:7.3 in line with the 2:9 stoichiometric ratio. Note that the cyanide signal displays a short tail toward lower binding energies, which may stem from the two different cyanides present in the molecule (at the bridge and in the terminal position), giving an asymmetrical peak. Finally, the Ru:N ratio found from the XPS signals and their corresponding atomic sensitivity factors yield 2:10, in good agreement with the expected ratio from the complex stoichiometry (2:11), indicating that the complex has been successfully anchored to the TiO_2 surface without decomposition. As typically seen in previous reports, the amount of carbon found on the surface exceeds the stoichiometric expected value by 30 %, as the methanol used for deposition may co-adsorb forming Ti-OCH_3 groups on the surface. Overall, XPS measurements of the dimer complex attached to the oxide surface confirm that adsorption occurs through the deprotonated carboxylic acid functional groups in a bidentate manner. The measured Ru:N ratio and the expected XPS features indicate that the complex is successfully anchored to the TiO_2 surface without decomposition and the single Ru $3d_{5/2}$ peak suggests electronic coupling between the Ru centers.

The geometric and electronic structure of the $[Ru(tpy)(dcb)\text{-}NC\text{-}(py)_4(CN)]^{2+}$ dimer adsorbed on TiO_2 (110) was further investigated using DFT calculations. Geometry optimizations were performed on the TiO_2 (110) supercell exploring various binding modes as described in Figure S17. Figure 7 presents the most stable configuration, where the

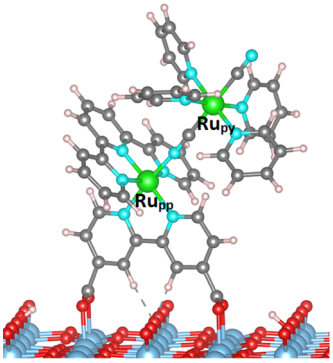

Figure 7. DFT optimized geometry for the adsorbed complex on the TiO_2 (110) surface. The coloring scheme for the molecule is O = red, Ru = green, N = light blue, C = gray, and H = pink.

complex is adsorbed in a deprotonated bidentate mode, with the resulting protons represented as surface hydroxyl groups in the model. Notably, the Ru_{py} atom is positioned further from the surface compared to Ru_{pp}, although they remain relatively close, with a separation of 0.52 and 1.18 and 0.79 nm from the TiO_2 surface plane, respectively. This configuration is consistent with the XPS measurements discussed above and with previous DFT studies of similar complexes adsorbed on TiO_2 (110), which also report comparable binding geometries, with deprotonated carboxylate groups binding to titanium atoms.[14,23] Consistent with this, the monomer Ru(dcb)(tpy)-CN binds to the TiO_2(110) surface in the same adsorption geometry.[23] Furthermore, adsorption of only the dcb ligand on TiO_2(110) also results in a deprotonated bidentate mode,[58] suggesting that the ligand governs the adsorption geometry of the molecular complex.

In order to explore the electronic structure of the Ru complex adsorbed on TiO_2(110), we calculated the density of states (DOS) for the system. Figure 8a shows the total DOS for the biruthenium complex on TiO_2(110), along with the projected density of states (PDOS) for the dimer complex, specifically highlighting the Ru 4d atomic orbitals. The occupied states cover a wide energy range (~24 eV), but we focus on those near the Fermi energy, as they are most relevant to the behavior of the adsorbed complex. Two distinct peaks associated with the Ru 4d states (green line) appear just below the band gap. The higher-energy peak is primarily attributed to the Ru_{py} states (the Ru atom furthest from the surface, as shown in Figure 7), while the lower-energy peak corresponds to the Ru_{pp} states. This energy ordering mirrors that observed in solution, where the Ru_{pp} states are more stabilized than the Ru_{py} states (Table S2). The highest occupied molecular orbital (HOMO) is composed of Ru 4d orbitals from both fragments delocalized over the bridge, while the lowest unoccupied molecular orbital (LUMO) is primarily delocalized over the π^* orbitals of the tpy ligand. Notably, the LUMO aligns energetically with the bottom of the conduction band. The spatial distributions of the HOMO and LUMO are shown in Figure 8b. As discussed previously, this configuration suggests the presence of a metal-to-ligand charge transfer (MLCT) excited state localized on the {Ru(tpy)} fragment near the surface. Although the LUMO is centered on the tpy ligand, it lies very close in energy to an orbital centered on the dcb ligand anchoring the complex (also shown in Figure 8b). It is expected that the initial excited state populated by the MLCT transition may decay to either orbital. The proximity of this orbital to the surface, combined with its energetic overlap with the bottom of the conduction band, enhances electronic coupling with the TiO_2 surface, lowers the activation barrier for electron injection into the conduction band, and facilitates efficient and rapid electron transfer.

CONCLUSIONS

We have examined the interaction of a cyanide-bridged biruthenium complex with rutile TiO_2(110) surfaces using XPS and DFT calculations. Our results demonstrate that the dimer complex binds to the TiO_2 surface in a bidentate configuration, with deprotonated carboxyl groups forming covalent bonds, similar to previously studied monomeric complexes. XPS data confirm that the dimer forms a stable monolayer, covering approximately 50% of the surface area. Also, the complex shows a high degree of electronic coupling, evidenced experimentally by the single Ru $3d_{5/2}$ XPS signal. Although DFT calculations of the [II,II] species indicate that the LUMO is localized on the tpy ligand, this orbital lies very close in energy to another orbital centered on the dcb ligand anchoring the complex to the TiO_2 surface. The proximity of this orbital to the surface, combined with the energetic alignment with the bottom of the conduction band, supports electron injection from the excited state of the complex into the semiconductor—a crucial step for efficient charge transfer processes in photocatalytic applications. For the mixed-valence state, DFT calculations in solution reveal that the hole is localized on the distal ruthenium center (Ru_{py}). Since this localization is driven by the higher basicity of the py ligand, we assume that the hole remains on Ru_{py} when the complex is adsorbed, keeping it spatially separated from the TiO_2/

https://doi.org/10.1021/acs.jpcc.5c01952
J. Phys. Chem. C XXXX, XXX, XXX−XXX

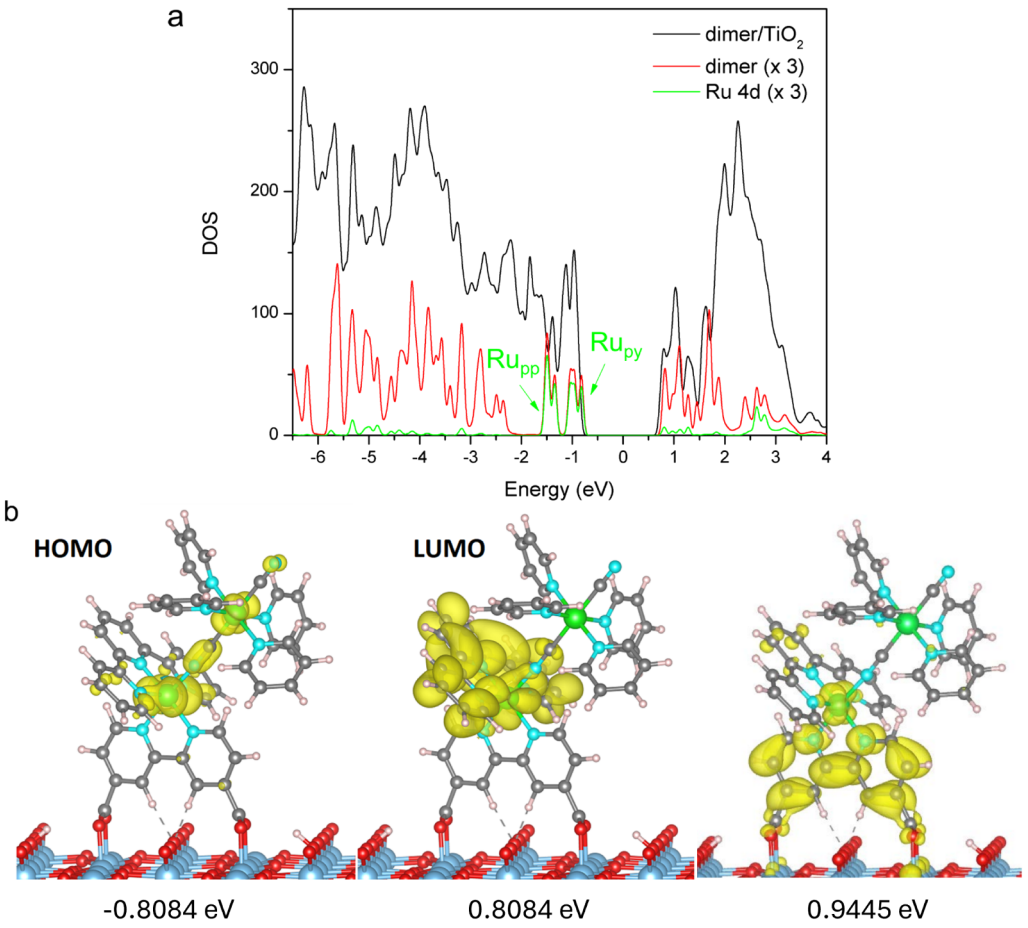

Figure 8. (a) DOS curves for the adsorbed complex on the TiO_2 (110) surface. Total DOS (black line), PDOS on the adsorbed complex (red line), and PDOS on the Ru 4d atomic orbitals (green lines) are included (PDOS were multiplied by a factor of 3). (b) HOMO, LUMO, and orbital centered on the dcb ligand of the adsorbed complex on the TiO_2 (110) surface.

complex interface. This distance likely reduces the rate of back-electron transfer from the surface to the mixed-valence complex, thus enhancing the stability of the charge-separated state and potentially improving the efficiency of photoelectrochemical processes. These findings provide valuable insights into the adsorption behavior and electronic interactions of biruthenium complexes on TiO_2 surfaces, which are important for developing advanced molecular systems for applications such as dye-sensitized solar cells and photocatalytic energy conversion.

■ ASSOCIATED CONTENT

Supporting Information

The Supporting Information is available free of charge at https://pubs.acs.org/doi/10.1021/acs.jpcc.5c01952.

Synthesis and characterization of $[Ru(tpy)(dcb)\text{-}NC\text{-}Ru(py)_4CN](PF_6)_2$; TD-DFT-calculated UV−vis transitions; C 1s and Ru 3d of $[Ru(tpy)(dcb)NCCH_3](PF_6)_2$ and $[Ru(tpy)(dcb)\text{-}NC\text{-}Ru(py)_4CN](PF_6)_2$ adsorbed on TiO_2(110) and C 1s and Ru 3d XPS spectra of solid $[Ru(tpy)(dcb)\text{-}NC\text{-}Ru(py)_4CN](PF_6)_2$, $Ru(py)_4(CN)_2$, and $[Ru(tpy)(dcb)NCS]PF_6$ (PDF)

■ AUTHOR INFORMATION

Corresponding Author

Federico J. Williams − *Departamento de Química Inorgánica, Analítica y Química Física, Facultad de Ciencias Exactas y Naturales, Universidad de Buenos Aires, Buenos Aires C1428EHA, Argentina; Instituto de Química Física de los Materiales, Medio Ambiente y Energía, CONICET-Universidad de Buenos Aires, Buenos Aires C1428EHA, Argentina;* orcid.org/0000-0002-6194-2734; Phone: +54 11 5285 8289; Email: fwilliams@qi.fcen.uba.ar

Authors

Luciano Sanchez Merlinsky − *Departamento de Química Inorgánica, Analítica y Química Física, Facultad de Ciencias Exactas y Naturales, Universidad de Buenos Aires, Buenos Aires C1428EHA, Argentina; Instituto de Química Física de los Materiales, Medio Ambiente y Energía, CONICET-Universidad de Buenos Aires, Buenos Aires C1428EHA, Argentina*

Bruno M. Aramburu-Trošelj − *Departamento de Química Inorgánica, Analítica y Química Física, Facultad de Ciencias Exactas y Naturales, Universidad de Buenos Aires, Buenos Aires C1428EHA, Argentina; Instituto de Química Física de los Materiales, Medio Ambiente y Energía, CONICET-Universidad de Buenos Aires, Buenos Aires C1428EHA, Argentina*

https://doi.org/10.1021/acs.jpcc.5c01952
J. Phys. Chem. C XXXX, XXX, XXX−XXX

Carolina Pistonesi − *Instituto de Física del Sur (IFISUR), Departamento de Física, Universidad Nacional del Sur, CONICET, Bahía Blanca B8000CPB, Argentina*

M. Estela Pronsato − *Instituto de Física del Sur (IFISUR), Departamento de Física, Universidad Nacional del Sur, CONICET, Bahía Blanca B8000CPB, Argentina*

Luis Baraldo − *Departamento de Química Inorgánica, Analítica y Química Física, Facultad de Ciencias Exactas y Naturales, Universidad de Buenos Aires, Buenos Aires C1428EHA, Argentina; Instituto de Química Física de los Materiales, Medio Ambiente y Energía, CONICET-Universidad de Buenos Aires, Buenos Aires C1428EHA, Argentina;* orcid.org/0000-0003-0666-5540

Complete contact information is available at: https://pubs.acs.org/10.1021/acs.jpcc.5c01952

Notes

The authors declare no competing financial interest.

■ ACKNOWLEDGMENTS

L.S.M. thanks CONICET for a doctoral scholarship. This work was supported by the Agencia Nacional de Promoción de la Investigación el Desarrollo Tecnológico y la Innovación (PICT 2018-03276), Universidad de Buenos Aires (UBACyT 2020), and CONICET (PIP 2021-2023).

■ REFERENCES

(1) Ashford, D. L.; Gish, M. K.; Vannucci, A. K.; Brennaman, M. K.; Templeton, J. L.; Papanikolas, J. M.; Meyer, T. J. Molecular Chromophore−Catalyst Assemblies for Solar Fuel Applications. *Chem. Rev.* **2015**, *115* (23), 13006−13049.

(2) Grätzel, M. Recent Advances in Sensitized Mesoscopic Solar Cells. *Acc. Chem. Res.* **2009**, *42* (11), 1788−1798.

(3) Balzani, V.; Bergamini, G.; Ceroni, P. From the Photochemistry of Coordination Compounds to Light-Powered Nanoscale Devices and Machines. *Coord. Chem. Rev.* **2008**, *252* (23−24), 2456−2469.

(4) Benniston, A. C.; Zeng, L. Recent Advances in Photorelease Complexes for Therapeutic Applications. *Dalton Trans.* **2022**, *51* (11), 4202−4212.

(5) O'Regan, B.; Grätzel, M. A. Low-Cost, High-Efficiency Solar Cell Based on Dye-Sensitized Colloidal TiO2 Films. *Nature* **1991**, *353* (6346), 737−740.

(6) Ardo, S.; Meyer, G. J. Photodriven Heterogeneous Charge Transfer with Transition-Metal Compounds Anchored to TiO_2 Semiconductor Surfaces. *Chem. Soc. Rev.* **2009**, *38* (1), 115−164.

(7) Pieslinger, G. E.; Albores, P.; Slep, L. D.; Coe, B. J.; Timpson, C. J.; Baraldo, L. M. Communication between Remote Moieties in Linear Ru−Ru−Ru Trimetallic Cyanide-Bridged Complexes. *Inorg. Chem.* **2013**, *52* (6), 2906−2917.

(8) Pieslinger, G. E.; Aramburu-Trošelj, B. M.; Cadranel, A.; Baraldo, L. M. Influence of the Electronic Configuration in the Properties of $d^6 - d^5$ Mixed-Valence Complexes. *Inorg. Chem.* **2014**, *53* (16), 8221−8229.

(9) Campagna, S.; Puntoriero, F.; Nastasi, F.; Bergamini, G.; Balzani, V. Photochemistry and Photophysics of Coordination Compounds: Ruthenium. In *Photochemistry and Photophysics of Coordination Compounds I*, Balzani, V.; Campagna, S., Eds.; Springer: Berlin Heidelberg, 2007; Vol. *280*, pp. 117−214. DOI: .

(10) Chiorboli, C.; Indelli, M. T.; Scandola, F. Photoinduced Electron/Energy Transfer Across Molecular Bridges in Binuclear Metal Complexes. In *Molecular Wires and Electronics*, Topics in Current Chemistry; Springer: Berlin, Heidelberg, 2005; Vol. *257*, pp. 63−102. DOI: .

(11) Kobayashi, A.; Takizawa, S.; Hirahara, M. Photofunctional Molecular Assembly for Artificial Photosynthesis: Beyond a Simple Dye Sensitization Strategy. *Coord. Chem. Rev.* **2022**, *467*, 214624.

(12) Wang, D.; Xu, Z.; Sheridan, M. V.; Concepcion, J. J.; Li, F.; Lian, T.; Meyer, T. J. Photodriven Water Oxidation Initiated by a Surface Bound Chromophore-Donor-Catalyst Assembly. *Chem. Sci.* **2021**, *12* (43), 14441−14450.

(13) Renz, M.; Kaupp, M. Predicting the Localized/Delocalized Character of Mixed-Valence Diquinone Radical Anions. Toward the Right Answer for the Right Reason. *J. Phys. Chem. A* **2012**, *116* (43), 10629−10637.

(14) Labat, F.; Ciofini, I.; Hratchian, H. P.; Frisch, M. J.; Raghavachari, K.; Adamo, C. Insights into Working Principles of Ruthenium Polypyridyl Dye-Sensitized Solar Cells from First Principles Modeling. *J. Phys. Chem. C* **2011**, *115* (10), 4297−4306.

(15) Schiffmann, F.; VandeVondele, J.; Hutter, J.; Wirz, R.; Urakawa, A.; Baiker, A. Protonation-Dependent Binding of Ruthenium Bipyridyl Complexes to the Anatase(101) Surface. *J. Phys. Chem. C* **2010**, *114* (18), 8398−8404.

(16) De Angelis, F.; Fantacci, S.; Selloni, A.; Nazeeruddin, M. K.; Grätzel, M. First-Principles Modeling of the Adsorption Geometry and Electronic Structure of Ru(II) Dyes on Extended TiO_2 Substrates for Dye-Sensitized Solar Cell Applications. *J. Phys. Chem. C* **2010**, *114* (13), 6054−6061.

(17) Hahlin, M.; Johansson, E. M. J.; Plogmaker, S.; Odelius, M.; Hagberg, D. P.; Sun, L.; Siegbahn, H.; Rensmo, H. Electronic and Molecular Structures of Organic Dye/TiO2 Interfaces for Solar Cell Applications: A Core Level Photoelectron Spectroscopy Study. *Phys. Chem. Chem. Phys.* **2010**, *12* (7), 1507.

(18) Oscarsson, J.; Hahlin, M.; Johansson, E. M. J.; Eriksson, S. K.; Lindblad, R.; Eriksson, A. I. K.; Zia, A.; Siegbahn, H.; Rensmo, H. Coadsorption of Dye Molecules at TiO_2 Surfaces: A Photoelectron Spectroscopy Study. *J. Phys. Chem. C* **2016**, *120* (23), 12484−12494.

(19) Johansson, E. M. J.; Hedlund, M.; Siegbahn, H.; Rensmo, H. Electronic and Molecular Surface Structure of $Ru(Tcterpy)(NCS)_3$ and $Ru(Dcbpy)_2(NCS)_2$ Adsorbed from Solution onto Nanostructured TiO_2: A Photoelectron Spectroscopy Study. *J. Phys. Chem. B* **2005**, *109* (47), 22256−22263.

(20) Westermark, K.; Rensmo, H.; Lees, A. C.; Vos, J. G.; Siegbahn, H. Electron Spectroscopic Studies of Bis-(2,2′-Bipyridine)-(4,4′-Dicarboxy-2,2′-Bipyridine)-Ruthenium(II) and Bis-(2,2′-Bipyridine)-(4,4′-Dicarboxy-2,2′-Bipyridine)-Osmium(II) Adsorbed on Nanostructured TiO_2 and ZnO Surfaces. *J. Phys. Chem. B* **2002**, *106* (39), 10108−10113.

(21) Westermark, K.; Henningsson, A.; Rensmo, H.; Södergren, S.; Siegbahn, H.; Hagfeldt, A. Determination of the Electronic Density of States at a Nanostructured TiO2/Ru-Dye/Electrolyte Interface by Means of Photoelectron Spectroscopy. *Chem. Phys.* **2002**, *285* (1), 157−165.

(22) Rensmo, H.; Westermark, K.; Södergren, S.; Kohle, O.; Persson, P.; Lunell, S.; Siegbahn, H. XPS Studies of Ru-Polypyridine Complexes for Solar Cell Applications. *J. Chem. Phys.* **1999**, *111* (6), 2744−2750.

(23) Merlinsky, L. S.; Pistonesi, C.; Pronsato, M. E.; Baraldo, L.; Williams, F. J. Electronic Structure Modulation in Ruthenium (II) Polypyridine Complexes Adsorbed on Rutile TiO2(110) Surfaces. *Surf. Sci.* **2024**, *742*, 122452.

(24) Weston, M.; Reade, T. J.; Handrup, K.; Champness, N. R.; O'Shea, J. N. Adsorption of Dipyrrin-Based Dye Complexes on a Rutile TiO_2 (110) Surface. *J. Phys. Chem. C* **2012**, *116* (34), 18184−18192.

(25) Mayor, L. C.; Ben Taylor, J.; Magnano, G.; Rienzo, A.; Satterley, C. J.; O'Shea, J. N.; Schnadt, J. Photoemission, Resonant Photoemission, and x-Ray Absorption of a Ru(II) Complex Adsorbed on Rutile TiO2(110) Prepared by *in Situ* Electrospray Deposition. *J. Chem. Phys.* **2008**, *129* (11), 114701.

(26) Varughese, B.; Chellamma, S.; Lieberman, M. XPS Study of Self-Assembly of Ruthenium Dimers $[((Acac)_2Ru)_2Bptz]^{0,+}$ on Hydrophobic and Hydrophilic SAMs. *Langmuir* **2002**, *18* (21), 7964−7970.

(27) Armarego, W. L. F.; Perrin, D. D. *Purification of Laboratory Chemicals*, 4th ed.; Butterworth-Heinemann: Oxford, 2002.

(28) Williams, D. B. G.; Lawton, M. Drying of Organic Solvents: Quantitative Evaluation of the Efficiency of Several Desiccants. *J. Org. Chem.* **2010**, *75* (24), 8351−8354.
(29) Kaim, W.; Fiedler, J. Spectroelectrochemistry: The Best of Two Worlds. *Chem. Soc. Rev.* **2009**, *38* (12), 3373.
(30) Méndez De Leo, L. P.; De La Llave, E.; Scherlis, D.; Williams, F. J. Molecular and Electronic Structure of Electroactive Self-Assembled Monolayers. *J. Chem. Phys.* **2013**, *138* (11), 114707.
(31) Frisch, M. J.; Trucks, G. W.; Schlegel, H. B.; Scuseria, G. E.; Robb, M. A.; Cheeseman, J. R.; Scalmani, G.; Barone, V.; Mennucci, B.; Petersson, G. A. et al. *Gaussian 09, Revision D.01*; Gaussian INC, 2009.
(32) Szabo, A.; Ostlund, N. S. *Modern Quantum Chemistry: introduction to Advanced Electronic Structure Theory*; Dover Publications, INC: Mineola, N.Y, 1996.
(33) Tomasi, J.; Mennucci, B.; Cammi, R. Quantum Mechanical Continuum Solvation Models. *Chem. Rev.* **2005**, *105* (8), 2999−3094.
(34) Scalmani, G.; Frisch, M. J. Continuous Surface Charge Polarizable Continuum Models of Solvation. *I. General Formalism. J. Chem. Phys.* **2010**, *132* (11), 114110.
(35) Schlegel, H. B. Optimization of Equilibrium Geometries and Transition Structures. *J. Comput. Chem.* **1982**, *3* (2), 214−218.
(36) Stratmann, R. E.; Scuseria, G. E.; Frisch, M. J. An Efficient Implementation of Time-Dependent Density-Functional Theory for the Calculation of Excitation Energies of Large Molecules. *J. Chem. Phys.* **1998**, *109* (19), 8218−8224.
(37) Petit, L.; Maldivi, P.; Adamo, C. Predictions of Optical Excitations in Transition-Metal Complexes with Time Dependent-Density Functional Theory: Influence of Basis Sets. *J. Chem. Theory Comput.* **2005**, *1* (5), 953−962.
(38) O'boyle, N. M.; Tenderholt, A. L.; Langner, K. M. Cclib: A Library for Package-independent Computational Chemistry Algorithms. *J. Comput. Chem.* **2008**, *29* (5), 839−845.
(39) Fernández, C. C.; Wechsler, D.; Lytken, O.; Steinrück, H.-P.; Williams, F. J. Self-Metalation of Monophosphonic Acid Tetraphenylporphyrin on TiO2(110)-(1 × 1). *Surf. Sci.* **2022**, *717*, 122005.
(40) De La Llave, E.; Clarenc, R.; Schiffrin, D. J.; Williams, F. J. Organization of Alkane Amines on a Gold Surface: Structure, Surface Dipole, and Electron Transfer. *J. Phys. Chem. C* **2014**, *118* (1), 468−475.
(41) Kresse, G.; Furthmüller, J. Efficient Iterative Schemes for *Ab Initio* Total-Energy Calculations Using a Plane-Wave Basis Set. *Phys. Rev. B* **1996**, *54* (16), 11169−11186.
(42) Kresse, G.; Furthmüller, J. Efficiency of Ab-Initio Total Energy Calculations for Metals and Semiconductors Using a Plane-Wave Basis Set. *Comput. Mater. Sci.* **1996**, *6* (1), 15−50.
(43) Kresse, G.; Hafner, J. *Ab Initio* Molecular Dynamics for Liquid Metals. *Phys. Rev. B* **1993**, *47* (1), 558−561.
(44) Blöchl, P. E. Projector Augmented-Wave Method. *Phys. Rev. B* **1994**, *50* (24), 17953−17979.
(45) Perdew, J. P.; Burke, K.; Ernzerhof, M. Generalized Gradient Approximation Made Simple. *Phys. Rev. Lett.* **1996**, *77* (18), 3865−3868.
(46) Grimme, S. Semiempirical GGA-type Density Functional Constructed with a Long-range Dispersion Correction. *J. Comput. Chem.* **2006**, *27* (15), 1787−1799.
(47) German, E.; Faccio, R.; Mombrú, A. W. Comparison of Standard DFT and Hubbard-DFT Methods in Structural and Electronic Properties of TiO2 Polymorphs and H-Titanate Ultrathin Sheets for DSSC Application. *Appl. Surf. Sci.* **2018**, *428*, 118−123.
(48) Monkhorst, H. J.; Pack, J. D. Special Points for Brillouin-Zone Integrations. *Phys. Rev. B* **1976**, *13* (12), 5188−5192.
(49) Kavan, L.; Vlckova Zivcova, Z.; Zlamalova, M.; Zakeeruddin, S. M.; Grätzel, M. Electron-Selective Layers for Dye-Sensitized Solar Cells Based on TiO_2 and SnO_2. *J. Phys. Chem. C* **2020**, *124* (12), 6512−6521.
(50) Robin, M. B.; Day, P. Mixed Valence Chemistry-A Survey and Classification. *Adv. Inorg. Chem. Radiochem.* **1968**, *10*, 247−422.
(51) Demadis, K. D.; Hartshorn, C. M.; Meyer, T. J. The Localized-to-Delocalized Transition in Mixed-Valence Chemistry. *Chem. Rev.* **2001**, *101* (9), 2655−2686.
(52) Bangle, R. E.; Schneider, J.; Conroy, D. T.; Aramburu-Trošelj, B. M.; Meyer, G. J. Kinetic Evidence That the Solvent Barrier for Electron Transfer Is Absent in the Electric Double Layer. *J. Am. Chem. Soc.* **2020**, *142* (35), 14940−14946.
(53) Loague, Q.; Keller, N. D.; Müller, A. V.; Aramburu-Trošelj, B. M.; Bangle, R. E.; Schneider, J.; Sampaio, R. N.; Polo, A. S.; Meyer, G. J. Impact of Molecular Orientation on Lateral and Interfacial Electron Transfer at Oxide Interfaces. *ACS Appl. Mater. Interfaces* **2023**, *15* (28), 34249−34262.
(54) Aramburu-Trošelj, B. M.; Bangle, R. E.; Meyer, G. J. Solvent Influence on Non-Adiabatic Interfacial Electron Transfer at Conductive Oxide Electrolyte Interfaces. *J. Chem. Phys.* **2020**, *153* (13), 134702.
(55) Aramburu-Trošelj, B. M.; Oviedo, P. S.; Pieslinger, G. E.; Hodak, J. H.; Baraldo, L. M.; Guldi, D. M.; Cadranel, A. A Hole Delocalization Strategy: Photoinduced Mixed-Valence MLCT States Featuring Extended Lifetimes. *Inorg. Chem.* **2019**, *58* (16), 10898−10904.
(56) Wechsler, D.; Fernández, C. C.; Steinrück, H.-P.; Lytken, O.; Williams, F. J. Covalent Anchoring and Interfacial Reactions of Adsorbed Porphyrins on Rutile TiO_2 (110). *J. Phys. Chem. C* **2018**, *122* (8), 4480−4487.
(57) Balajka, J.; Hines, M. A.; DeBenedetti, W. J. I.; Komora, M.; Pavelec, J.; Schmid, M.; Diebold, U. High-Affinity Adsorption Leads to Molecularly Ordered Interfaces on TiO_2 in Air and Solution. *Science* **2018**, *361* (6404), 786−789.
(58) Patthey, L.; Rensmo, H.; Persson, P.; Westermark, K.; Vayssieres, L.; Stashans, A.; Petersson, Å.; Brühwiler, P. A.; Siegbahn, H.; Lunell, S.; Mårtensson, N. Adsorption of Bi-Isonicotinic Acid on Rutile TiO2(110). *J. Chem. Phys.* **1999**, *110* (12), 5913−5918.
(59) Wechsler, D.; Vensaus, P.; Tsud, N.; Steinrück, H.-P.; Lytken, O.; Williams, F. J. Surface Reactions and Electronic Structure of Carboxylic Acid Porphyrins Adsorbed on TiO_2 (110). *J. Phys. Chem. C* **2021**, *125* (12), 6708−6715.
(60) Shepherd, R. E.; Proctor, A.; Henderson, W. W.; Myser, T. K. Assessment of the.Pi.-Acceptor Capability of Selected Ligands Based on the Photoelectron Spectra of Ruthenium Ammine Complexes. *Inorg. Chem.* **1987**, *26* (15), 2440−2444.
(61) Cano, A.; Avila, Y.; Avila, M.; Reguera, E. Structural Information Contained in the XPS Spectra of Nd10 Metal Cyanides. *J. Solid State Chem.* **2019**, *276*, 339−344.

https://doi.org/10.1021/acs.jpcc.5c01952
J. Phys. Chem. C XXXX, XXX, XXX−XXX